Biochimica et Biophysica Acta 1838 (2014) 1710–1718

Contents lists available at ScienceDirect

Biochimica et Biophysica Acta

journal homepage: www.elsevier.com/locate/bbamem

Induced movements of giant vesicles by millimeter wave radiation

Martina Albini [a], Simone Dinarelli [b], Francesco Pennella [c], Stefania Romeo [d], Emiliano Zampetti [e], Marco Girasole [b], Umberto Morbiducci [c], Rita Massa [f], Alfonsina Ramundo-Orlando [a,*]

[a] IFT-CNR, 00133 Rome, Italy
[b] ISM-CNR, 00133 Rome, Italy
[c] Department of Mechanical and Aerospace Engineering, Politecnico di Torino, 10129 Turin, Italy
[d] IREA-CNR, 89124 Naples, Italy
[e] IMM-CNR, 00133 Rome, Italy
[f] Department of Physics, University Federico II, 89126 Naples, Italy

ARTICLE INFO

Article history:
Received 3 December 2013
Received in revised form 26 March 2014
Accepted 27 March 2014
Available online 4 April 2014

Keywords:
Giant vesicles
Vesicles trajectories
Movement changes
Millimeter waves
Non thermal mechanism
Real-time exposure

ABSTRACT

Our previous study of interaction between low intensity radiation at 53.37 GHz and cell-size system – such as giant vesicles – indicated that a vectorial movement of vesicles was induced. This effect among others, i.e. elongation, induced diffusion of fluorescent dye di-8-ANEPPS, and increased attractions between vesicles was attributed to the action of the field on charged and dipolar residues located at the membrane–water interface. In an attempt to improve the understanding on how millimeter wave radiation (MMW) can induce this movement we report here a real time evaluation of changes induced on the movement of giant vesicles. Direct optical observations of vesicles subjected to irradiation enabled the monitoring in real time of the response of vesicles. Changes of the direction of vesicle movement are demonstrated, which occur only during irradiation with a "switch on" of the effect. This MMW-induced effect was observed at a larger extent on giant vesicles prepared with negatively charged phospholipids. The monitoring of induced-by-irradiation temperature variation and numerical dosimetry indicate that the observed effects in vesicle movement cannot be attributed to local heating.

© 2014 Elsevier B.V. All rights reserved.

1. Introduction

The millimeter wave band is officially used in non-invasive complementary medicine in many Eastern European Countries against a variety of diseases such as cardiovascular disorders, diabetes, gastrointestinal disorders and also for pain relief [1–4]. The most common frequencies used are 42.2, 53.37, and 61.2 GHz, which are usually administered onto a localized area of the skin at a sufficiently low intensity such that there is no perceptible heating. However, no clear explanation of the mechanism underlying its effectiveness has been provided [5]. Recently also in Western Countries diagnostic and therapeutic medical applications of millimeter waves have been proposed [6,7].

On the other hand the interaction of millimeter waves (MMW) radiation with biological systems is a fundamental scientific topic of great interest. Vibrational dynamics in biochemical reactions of large macromolecules in living organisms play an important role in fundamental processes related for instance to the transfer of genetic information and protein interactions. Many of the vibration modes in complex biomolecules fall in the 1 GHz to 100 GHz range [8]. In this frequency range there are also significant parts of the intermolecular vibrational/librational modes of water, fluctuations of atoms in organic molecules and hydrogen bonds [9]. Therefore, biologically relevant processes can be initiated using radiation in this frequency domain.

Our previous study of interaction between low intensity radiation at 53.37 GHz and giant vesicles (GVs), demonstrated that non-random perturbation in the movement of the vesicles was induced only during irradiation with a "switch on" of the effect [10]. This effect among others, i.e. elongation, induced diffusion of fluorescent dye di-8-ANEPPS, and increased attraction between vesicles was attributed to the action of the field on charged and dipolar residues located at the membrane–water interface. This hypothesis seems to be reinforced by our recently obtained results on permeability increase induced on cationic lipid vesicles subjected to same low intensity radiation at 53.37 GHz [11].

With the purpose of improving the understanding on how this very low intensity radiation [12] can induce this movement, we report here a real time evaluation of directional changes induced on giant vesicles. These vesicles have a unique property: they are only a few tens of microns in size, as a consequence, they are visible under a light microscope and provide a handy biomimetic tool for displaying directly the response of the membrane on the cell-size scale. Furthermore, they have been already used successfully for investigating a wide range of events, including the static and dynamic behavior of membranes [13,14] and rheology and dynamics of red blood cells [15,16].

* Corresponding author at: Institute of Translational Pharmacology (IFT), National Research Council of Italy, Via del Fosso del Cavaliere, 100-00133 Rome, Italy. Tel.: +39 06 4548 8213; fax: +39 96 4548 8257.
E-mail address: alfonsina.ramundoorlando@ift.cnr.it (A. Ramundo-Orlando).

http://dx.doi.org/10.1016/j.bbamem.2014.03.021
0005-2736/© 2014 Elsevier B.V. All rights reserved.

The characterization of MMW radiation exposure conditions in terms of the field distribution in the liposome sample is fundamental to achieving information about the field level and any related thermal increase. Here the specific absorption rate (SAR) is evaluated and correlated with the observed effects in the vesicle movement. Furthermore, well-defined and characterized exposure conditions are provided in this study, as suggested in the literature, for obtaining adequate interpretation and reproducibility of the result [17].

In this report the motion of vesicles was investigated by processing images acquired by a correctly set optical system. Technically, a semi-automated strategy allowed evaluation of the perturbation noticed in vesicle motion by the turning on and off of the irradiation.

2. Materials and methods

2.1. Chemicals

L-α-Phosphatidylcholine (egg yolk PC) and phosphatidylglycerol sodium salt (PG) were purchased by Sigma Aldrich (St. Louis, MO). Spectroscopic grade organic solvents and pure distilled water were purchased from Carlo Erba Reagenti (Milano, Italy). Anhydrous, pro-analysis (p.a.) glucose and sucrose (Fluka Biochimica, Switzerland) were used without further purification.

2.2. Giant vesicles preparation

Giant vesicles were prepared from egg yolk PC using the electroformation method from lipid films spin-coated on 45 mm × 45 mm glass slide covered with indium tin oxide (ITO) [18]. Briefly, egg yolk PC was dissolved in chloroform:acetonitrile (95:5 v/v), at a concentration of 3.75 mg ml^{-1}. Approximately 0.25 ml of this solution was deposited on the conductive face of the ITO glass, and spin-coated at 600 rpm for 5 min (BLE Laboratory Equipment, GmBh). The lipid films were then dried under vacuum (~8 mbar) overnight to remove traces of solvent. The preparation chamber was made from two pieces of ITO glass, with their conductive faces facing each other, separated by a 1.6 mm thick rectangular frame of poly-dimethylsiloxane (PDMS), the whole held together with small binder clips. Solution of 0.2 M sucrose was injected through a hole in the PDMS spacer, and a voltage of 10 Hz 1.2 V peak-to-peak was immediately applied between the two ITO glasses. The formation of giant vesicles was then observed by light microscope. After approximately 1.5–2 h, vesicles of a size >30 μm in diameter were formed. The giant vesicles were detached from the ITO glass by the application of a voltage of 3 V peak-to-peak, 5 Hz for 10 min. The vesicles that were swollen in 0.2 M sucrose solution were recovered by gentle suction with a syringe, and were transferred to the wells of the exposure chamber, a four-dish polystyrene (NUNC Brand Products, Denmark), in a medium containing 0.2 M glucose solution. The sugar solutions inside and outside the vesicles were isotonic to prevent the vesicles from collapsing due to the osmotic difference across the membrane.

In some occasion to prepare anionic GV, mixtures of egg yolk PC and PG at molar ratio of 9:1 were used.

All steps of the vesicle preparations and exposures were performed at room temperature, which is above the main phase transition one of egg-PC, so that the phospholipids were in their liquid crystalline state.

2.3. Optical microscopy and movement analysis

Microscopy observations were performed on an Olympus (Rungis, France) IX 70 inverted microscope in phase contrast mode; the objective lens used was 20× with a total magnification of 200×.

Carefully attention was given to avoid any possible artifacts influencing the movements of GVs: To maintain system stability during growth and analysis, the microscope was placed on a Newport air-controlled vibration control table; the turning on–off of the microscope light, camera and millimeter wave antenna was governed by a unique push button placed on a well-separated table.

The microscope was equipped with an optical condenser and a high speed camera having a 1 kHz frame acquisition rate (F-View II — Soft Imaging System GmbH, Germany). Image recording was always performed at focal planes away from the top, bottom and sides of the dish. The microscope light was turned on only for the short time necessary for image acquisition. One image per minute was acquired, if not otherwise specified, along the entire time scale of the experiments by using the analysis control software. The microscope images were post-processed by using the open source software 'ImageJ' [19]. In detail, the plug-in MTrackJ was applied to obtain the sequence of coordinates indicating the position of each tracked vesicles at each time point. These results were imported into a Matlab environment where: (1) selected vesicle trajectories were reconstructed from the measured coordinates; (2) the angles between vectors connecting two consecutive points of the trajectory described by each vesicle during its motion and a reference direction (which was set as the horizontal one, corresponding to the x-axis of the reference coordinate system adopted here, as will be clear in the forthcoming Results section) — the so-called instantaneous angles [20] were evaluated; (3) polar plots of the distribution of instantaneous angular values were generated.

2.4. Millimeter waves exposures

An exposure chamber made of four separate dishes, which were devoid of any conductive materials, was placed on the microscope stage (Fig. 1). Each dish was filled with 1.5 ml of 0.2 M glucose solution. The dishes were processed separately, a small amount of giant vesicles (2–4 μl) being added prior to the irradiation, and carefully checked for level using a circular spirit level. For each GVs preparation a minimum of 5 samples was processed.

The experiments were performed at 53.37 GHz by using a conical horn antenna (IMG-53.37, Micro Med Tech, Russia) with 34 mm of maximal diameter (D) and an output power of 39 mW. The distance (R) of the center of the exposed dish from the horn antenna was 8 cm and the incidence angle was 45° (Fig. 2A). It is worth noticing that in this test bench configuration an upward irradiation is applied on the samples, which enhances the efficiency of the exposure due to the reduction

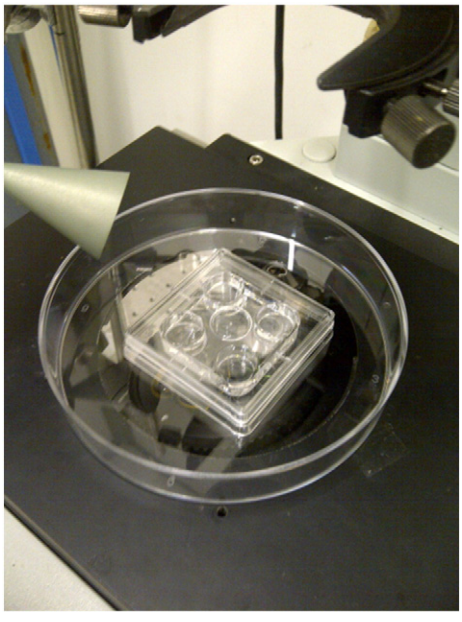

Fig. 1. MMW exposure chamber (polystyrene four dishes) on the microscope stage is shown.

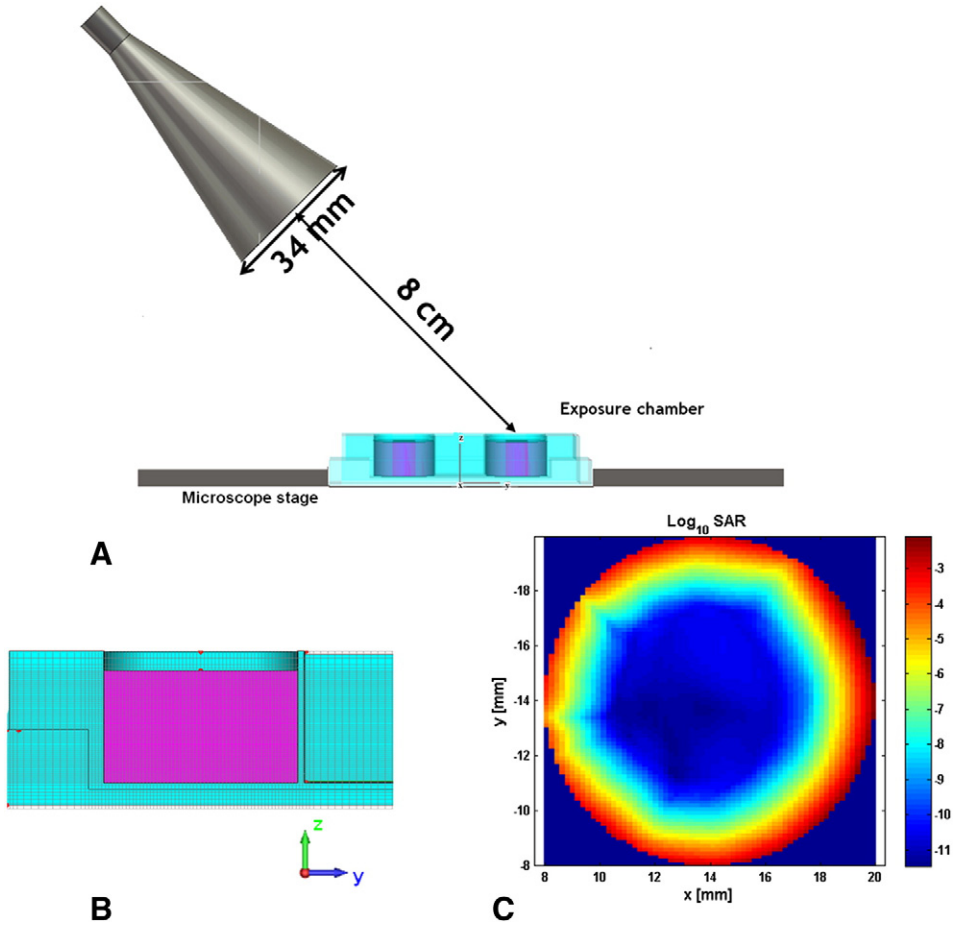

Fig. 2. Model of the experimental set up for exposure to 53.37 GHz including the horn antenna and the modeled exposure chamber. A) Side view: showing that the sample was exposed from the top. B) CAD model of dish (diameter of 15 mm and height of 8.5 mm). The grid mesh side view is shown. C) Top view of SAR distribution in the 41st mesh layer in the computational domain is shown.

of (1) the multiple reflections between the chamber and the horn antenna and (2) the field disturbance due to the wave reflections from the workbench [21].

The GVs suspension was subjected to either 53.37 GHz radiation or sham exposure, i.e., when the 53.57 GHz radiation was turned off. The irradiation was intermittently turned on and off at the time intervals indicated in Results and discussion section. The overall experimental setup was located in a temperature-controlled room, which governed the exposure temperature. Temperature measurements inside the samples were performed using a four-channel Analog Device electronic thermometer equipped with two Flexible Implantable Probes (Physitemp Instruments, Inc. Type IT-18) of 0.06 cm diameter, a lead length of 1 m, time constant of 0.1 s, and resolution of 0.01 °C. The probe tip of thermocouple was placed in the center of the dish, around 4 mm below the upper surface of the aqueous solution containing the vesicles, where microscope images were always collected.

2.5. Numerical dosimetry

To evaluate SAR distribution inside the exposure chamber a computational strategy was applied. The computational study was performed by applying a finite integration technique-based commercial code (CST Microwave Studio, Darmastadt, Germany), and a more accurate dosimetry than previously described [10] was performed. In particular, in the present study, the hypothesis of local plane incident wave was removed and the horn antenna was considered as MMW radiation source.

The circular horn antenna at 53.37 GHz and the dish containing the glucose solution sample – a perfectly cylindrical shape of diameter 15 mm and height of 8.5 mm – were considered and carefully designed (Fig. 2A–B) to facilitate calculating as realistically as possible (1) the electric field in the computational domain and (2) SAR distribution in the giant samples. The dielectric parameters of the materials adopted for the simulation at the working frequency are reported in Table 1.

An adaptive mesh tool was adopted for analyzing the entire domain. In detail, the modeled sample was subdivided into a computational grid in such a way that the dimension of each cell was about 1/10 of the wavelength λ, which in the aqueous samples is equal to 1.2 mm. As a consequence, the resulting computational domain was discretized into $0.145 \times 0.145 \times 0.145$ mm^3 grid cells, and over each node of the grid the electric field was calculated. The local SAR (W/Kg) was evaluated from the electric field by applying the formula:

$$\mathrm{SAR} = \frac{P_a}{m} = \frac{1}{2}\frac{\sigma}{\rho}|E|^2, \quad (1)$$

where P_a is the absorbed power, m the mass of the sample and E the local electric field amplitude. As the concentration of giant vesicle

Table 1
Dielectric parameters adopted in the numerical simulation.

Component	Materials	Relative dielectric constant	Effective electric conductivity [S/m]
Horn antenna	PEC	–	∞
Sample	Glucose solution	14	71.2
Dish	Polystyrene	2.4	–

suspensions is extremely low we made an assumption that the permittivity value is that of glucose solution at 53.37 GHz [22]. As a consequence, the adopted values for effective electric conductivity – σ – and skin depth – δ – were set equal to 71.2 S/m and 0.34 mm, respectively. As for mass density – ρ – the value of 0.2 M glucose solution 1010 kg/m3 was adopted [23].

The layer-by-layer SAR distribution was processed and the spatial average inside the modeled samples was evaluated in 85 mesh layers (Fig. 2B). Fig. 2C shows the SAR distribution in correspondence of the critical observed region, at around 4 mm below the upper surface of liquid (41st mesh layer in the computational domain).

3. Results and discussion

3.1. Formation of giant vesicles

Vesicles produced from spin-coated lipid films were unilamellar, uniform, spherical and with a mean diameter of 16 μm (Fig. 3). Girard and coworkers previously showed that GVs obtained through electroformation were unilamellar [24]. In the irradiation experiments, individual spherical vesicles of different size were selected with diameters ranging from 14 μm to 30 μm.

In all thirteen preparations of GVs used throughout this work we found that if the liquid suspensions containing the giant vesicles were maintained for more than 5 h, the vesicles did not grow further, neither did they collapse, indicating a good stability of vesicle preparations, a prerequisite for successful investigation of the effects induced by MMW radiation.

For enhancing the visualization of vesicles on microscope images the use of a diffraction index asymmetry, achieved by using solutions of sucrose inside and glucose outside the GVs, was, for us, preferential to fluorescent dyes, for instance di-8ANEPPS. In fact during MMW irradiation these dyes can diffuse resulting in a blurring of the vesicle edges making GVs observation more difficult [10]. In order to reduce the possible impact that the viscosity could have on the motion of vesicles, we also tried to use vesicles, containing 0.01 M sucrose solution and diluted in 0.01 M glucose solution, unfortunately observing them was difficult, and they moved away from the microscope's field of view in a short time making it difficult to perform sham and irradiation treatments on the same sample, a prerequisite of this study. Thus we decided to use the same concentration of sugar solutions as in the previous work [10].

3.2. Temperature measurements

To evaluate the heating effect of MMW irradiation, we carefully measured temperature changes in the liquid containing the vesicles. Because most of the incident MMW energy is absorbed within the first few one-tenths of a millimeter in liquid media [25], temperature gradients close to the irradiated surface can be high enough to produce different types of convection process. As a matter of fact, being the SAR also related to the rate of temperature increase ($SAR = c_p\,(\Delta T/\Delta t)$), where c_p is the specific heat capacity of 0.2 M glucose solution, $c_p = 4101$ J/kg K [26] and ΔT is the temperature increase observed over a time interval Δt, the layer-by-layer, average thermal increase has been calculated in the exposed sample as a result of the numerical dosimetry. As shown in Fig. 4, a very steep thermal gradient occurs in the first few tenths of a mm ($\approx\delta = 0.34$ mm) from the top surface of the sample. However, it must be pointed out that such a relation does not take into account any thermal conductive and convective exchanges.

Since GVs were randomly dispersed in the glucose solution at layers well below the upper surface of the liquid we studied the behavior of temperature dynamics in samples subjected to a time-interrupted regime of exposure, positioning the thermocouple probe tip away from the top, bottom and sides of the dish. A typical example of the temperature dynamics recorded during these exposure experiments is shown in Fig. 5. The average temperature increase achieved on three different samples after 20 min of interrupted regime of exposure (MMW off for 5 min then on for 5 min then off for 5 min, and then on for 5 min) was 0.15 ± 0.05 °C. This weak temperature increase inside the irradiated sample could be ascribed to the unavoidable SAR difference between the boundaries and the bulk, which takes origin in the low penetration depth of MMW. However, such a temperature increase is considered in the literature to be below the threshold at which its effects should be considered thermal [27,28]. No further temperature increments were observed when the microscope light was turned on for the time necessary to acquire the images (data not shown), indicating that no marked temperature elevation was created under our exposure conditions.

3.3. Millimeter wave irradiation

In order to evaluate the effects of irradiation, vesicles were selected one at a time following the criteria that they were not connected to others and did not have internal formations or visible protuberances, as suggested elsewhere [29]. The concentration of vesicles was maintained sufficiently low such that they could move in the solution freely and without collision.

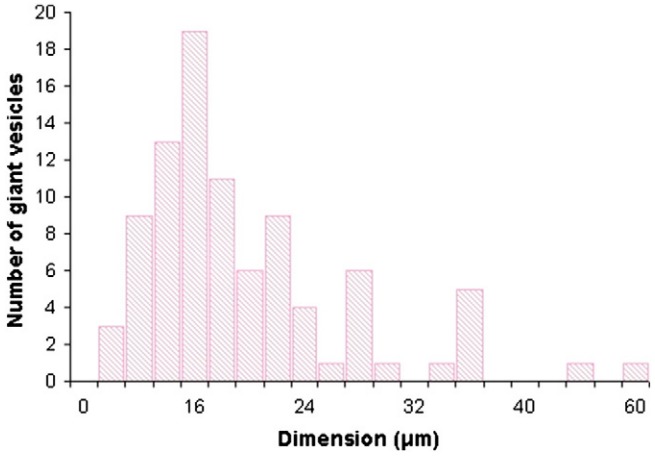

Fig. 3. Size distribution of GVs on four different preparations. In the irradiation experiments, individual spherical vesicles of different size were selected with diameters from 14 μm to 30 μm.

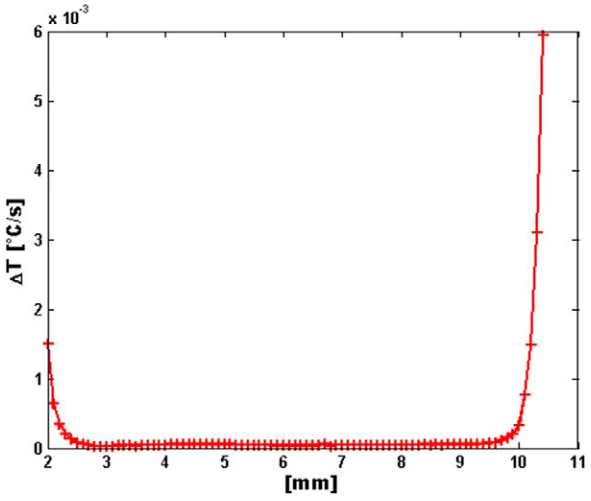

Fig. 4. Modeled rate of thermal increase in the exposed sample as derived from SAR calculation being the temperature rise ($\Delta T/\Delta t$) proportional to SAR.

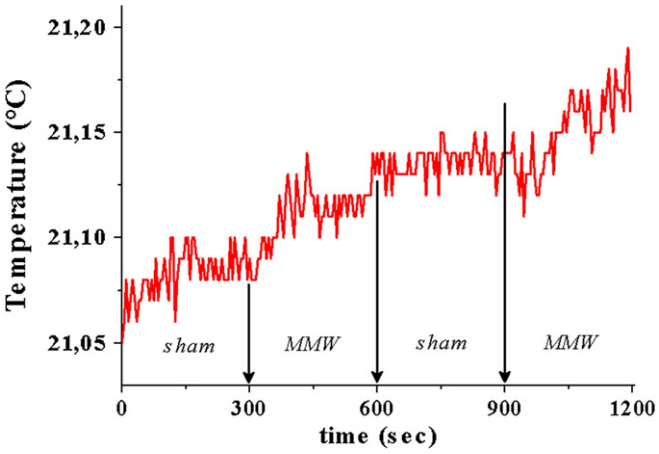

Fig. 5. Temperature dynamics recorded in a sample subjected to a typical time-interrupted regime of exposure (MMW was off for 5 min, then on for 5 min, then off for 5 min, and then on for 5 min). The probe tip of thermocouple was positioned in the center of the dish at around 4 mm below the upper surface of the aqueous solution containing the vesicles. The point at which the irradiation was turned on is marked with arrows.

In a first attempt, the visual inspection of the acquired video recording of vesicle dynamics in sham condition (i.e. when the 53.57 GHz radiation was turned off) revealed that GVs usually moved randomly away from the microscope's field of view during 20 min of observation by exhibiting not preferential directions in lateral displacements. Based on this finding, the maximum observation time adopted during irradiation experiments was usually never more than that.

To provide an experimental control with microscope light turned on only for the short time needed for image's acquisition, vesicle movement was analyzed on three different samples. The resultant sequence of microscope images collected during the sham condition was processed to track vesicle motion in the image plane. Fig. 6A shows a representative microscope image with two vesicle trajectories overlaid. In this specific case eleven microscope images were acquired and analyzed for the trajectories related to two individual vesicles. In the absence of irradiation, vesicle motion is driven essentially by mechanical force fields, such as gravity, buoyancy or diffusion. In particular, due to the action of the gravitational force, the observed phenomenon can be ascribed mainly to a sedimentation process. A not unidirectional correlated motion of the vesicles was observed (a similar behavior was observed in all sham samples). This correlated motion could be interpreted as a possible artifact influencing the motion of vesicles. Nevertheless, given that the experimental setup was carefully controlled, especially for level, we do not expect this to be the case. Neither the influence of electrostatic interactions between different components in our experimental setup, due to the absence of charged glass substrate or ionic conditions, can be considered. These electrostatic interactions may affect the behavior of a suspended vesicle, for instance, in determining the sedimentation dynamics of the vesicle.

The literature does not report clear evidence of highly correlated motion characterized by lateral displacements in the sedimentation process of (sham) vesicles as in Fig. 6A. However, in a very recent study it is mentioned that vesicles in isotonic conditions present significant lateral displacements during sedimentation process [30]. This observation could be taken to support our findings.

Further, a possible explanation of our findings could be found in the onset of deformation in vesicle membrane. It has been shown [31] that membrane deformation in a sedimentation process is caused by superimposition of two modes: smoothing of thermal undulations and direct stretching of the membrane. At low external forces (as in our sham condition), it is expected that strain should be due to the former mode only. Hence, vesicles of similar dimensions undergoing sedimentation process, in the same small region, are subjected to similar deformations, which, in turn, could dictate similar deflection from trajectories aligned to the direction of action of the external force, which in our condition should be the gravitational force.

Fig. 6B shows the angular histogram of the distribution of instantaneous angular values of these two vesicles. The observed distribution of angles confirms that, in the absence of irradiation, the vesicles moved spanning a wide range of deflection angles describing their trajectory. For the sake of completeness, we report here, that the overall occurrence of −x or +x direction of deflection in vesicle motion is almost the same in all the sham samples observed.

Surprisingly, in two different GV preparations we always observed vesicles exhibiting collective changes in the direction of movement when MMW radiation was switched on. Fig. 7 shows a representative example of different angles of the direction of a vesicle movement, calculated on trajectories of images acquired during sham (MMW off for 5 min) and irradiation (MMW on for 5 min) condition.

To ascertain if the MMW-induced effect on GVs movement would be directional, the trajectories of vesicles subjected to a time-interrupted regime of exposure (MMW off for 5 min, then on for 5 min, then off for 5 min, and then on for 5 min) were analyzed on a further six different GV preparations. A representative example of the results of the analysis is shown in Fig. 8, where the trajectories related to six individual

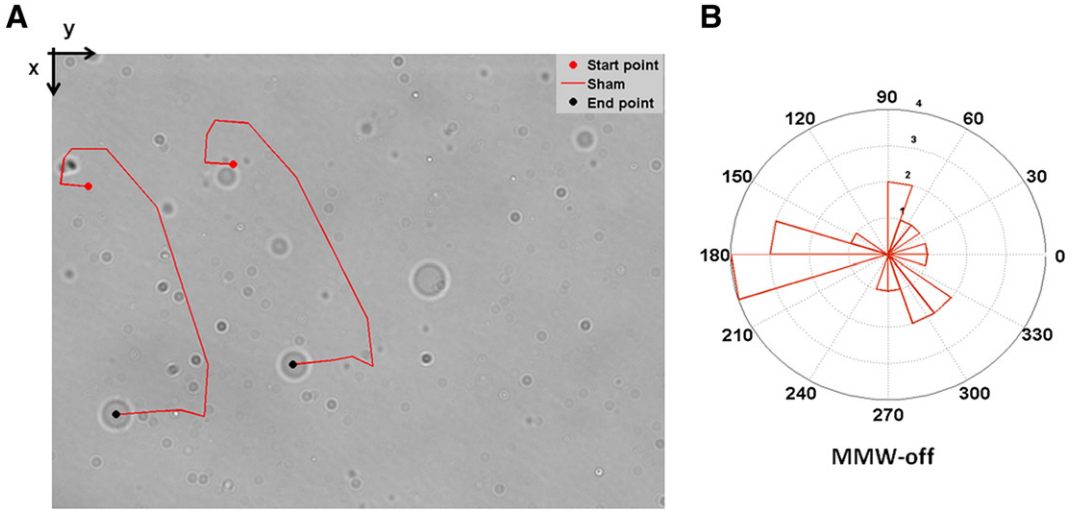

Fig. 6. Analysis of vesicle trajectory of sample not subjected to irradiation (sham). A) Eleven microscope images were acquired and analyzed for the trajectories related to two individual vesicles (diameters from 14 μm to 20 μm). B) Plots angular histogram of the distribution of instantaneous angular values.

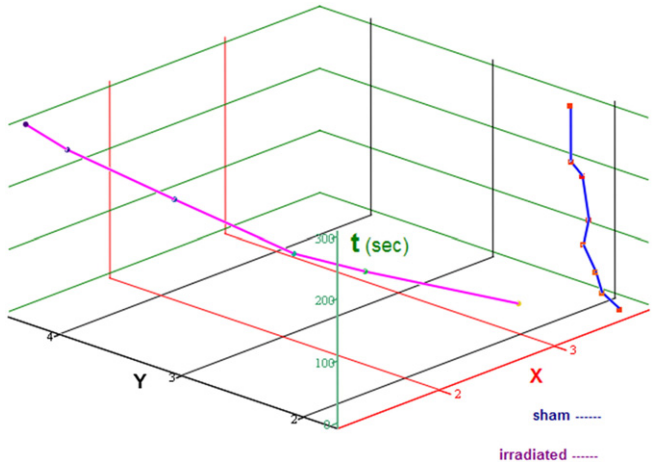

Fig. 7. A 3D plot of the movements in the XY plane of sham — blue – and irradiated — violet-vesicles with respect to elapsed time — the green vertical axis.

vesicles are presented. It can be observed that all vesicles are characterized by similar trajectories during irradiation independently from their dimensions. Notably, marked changes in the orientation of vesicle trajectories occurred only at the MMW-switch on and not at MMW-switch off, indicating that the influence of irradiation was determinant in eliciting the effect.

There is evidence of the presence of instability of a vesicle membrane driven by electromagnetic fields due to a reorganization of charges both internal and external to the vesicle. It has been shown [32,33] that the vesicle shape is obtained by balancing electric, hydrodynamic, bending and tension stresses exerted on the membrane and describe the time evolution of the transient vesicle deformation. In our case a similar transient deformation of the vesicles could, in principle, result and contribute to the observed changes in direction of the GVs when the MMW is turned on, with a reversed deflection in the trajectories when the MMW is applied a second time. On the other hand, the time scale of these phenomena is orders of magnitude smaller than the observation times of our study and the image resolution we used to depict vesicle motion does not allow observing small shape deformations. However, it should be mentioned here, that there is still no evidence

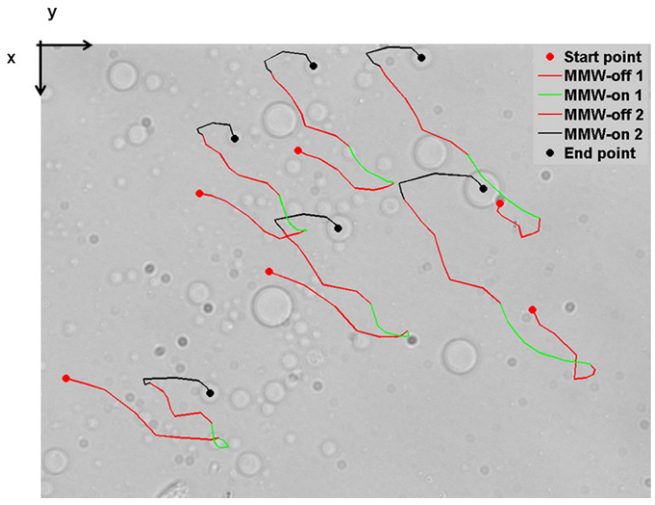

Fig. 8. Analysis of vesicle trajectory of sample subjected to interrupted regime of exposure as in Fig. 5. Twenty-nine microscope images were acquired and analyzed for the trajectories related to six individual vesicles (diameters from 14 μm to 30 μm). The green and black segments exhibit MMW treatment and the red segment is sham condition.

that, e.g., AC electric fields in the range of frequency of millimeter waves could lead to deformations in the shape of the vesicles [34].

Fig. 9A–D shows the angular histograms of the distribution of instantaneous angular values, related to the trajectories described from these six vesicles during the four phases of the exposure. The vesicles clearly moved from +x to –x at the first MMW-switch on (Fig. 9A versus B) and again from –x to +x at the second MMW-switch on, the latter case being characterized by a biphasic distribution (Fig. 9C versus D).

Remarkably, when the MMW was turned off during the intermediate period of sham condition (Fig. 9C), no change in angular distribution was observed, indicating that the strong alignment imposed on vesicle movement as a consequence of the previous 5 min of irradiation (Fig. 9B) is maintained. This could be probably ascribed to inertial effects in vesicle motion within the liquid.

When another sample was subjected to a shorter period of radiation (MMW off for 5 min, on 1 min, off 5 min) no marked changes in the orientation of vesicle motion was observed (data not shown). These findings lead us to conjecture that the duration of irradiation (accumulation effects?) could play a role in the orientation changes in vesicle's motion and also that they confirm the switch on/off character of the MMW-induced effects.

In the previous study [10], we hypothesized that GVs, even if they do not couple to the electromagnetic fields with sufficient strength to allow significant energy transfers [35], exhibited physical changes – including in their movement – due to the action of MMW at the membrane–water interface, where charged and dipolar residues are located (i.e., the zwitterionic phosphocholine headgroup and/or the first layer(s) of bound water molecules).

To further investigate this assumption, we used GVs prepared with a mixture of electrically neutral phosphatidylcholine – egg yolk PC – and a representative of negatively charged phospholipids, such as phosphatidylglycerol. The preparation of GVs is efficiently improved if their lipid composition includes PG [36]. The use of negatively charged phospholipids, e.g., phosphatidylserine or inositol phospholipids other than PG, has its rationale in the fact that they are always contained in biological membranes and play many important roles in living cells.

Surprisingly, negatively charged GVs in a sham condition moved away from the microscope's field of view in an overall time shorter than neutral ones. Thus the maximum observation time has to be reduced. The vesicle trajectories were analyzed on six different samples subjected to a time-interrupted regime of exposure of MMW off for 5 min, then on for 2 min and 30 s, then off for 1 min, then on for 5 min, and then off for 3 min.

Fig. 10 shows a representative example in which a sequence of eighteen acquired microscope images was used to analyze the trajectories of three individual vesicles; for various reasons it was not possible to track them for the entire time of their treatment. However, since vesicles have similar trajectories during irradiation, taken together the overall analysis revealed again significant changes of direction at the MMW-switch on and not at MMW-switch off.

Remarkably, the charged vesicles present the peculiarity that their movement is restricted within the –x portion of the polar plot and the main change of direction was toward the antenna side (Fig. 11C versus D). A possible explanation for differences observed in the movement of charged and non-charged GVs could be in the different distribution of the charge (1) internal to the vesicle membrane and (2) between the internal and external of the membrane [34]. From our findings, we conjecture that charged GVs experience an increase in their velocity in the switch-on phase and the onset of more marked inertial effects in the switch-off phase (which are the consequence of the increased velocity). The action of inertial effects is supported by the observed lack of relevant changes in the direction of the motion of charged GVs after the switch-off (Fig. 11B versus C). This behavior was not observed in non-charged GVs (Fig. 9B versus C).

In addition simulation data demonstrated that, as expected, due to the high conductivity of the water, higher SAR values resulted at the

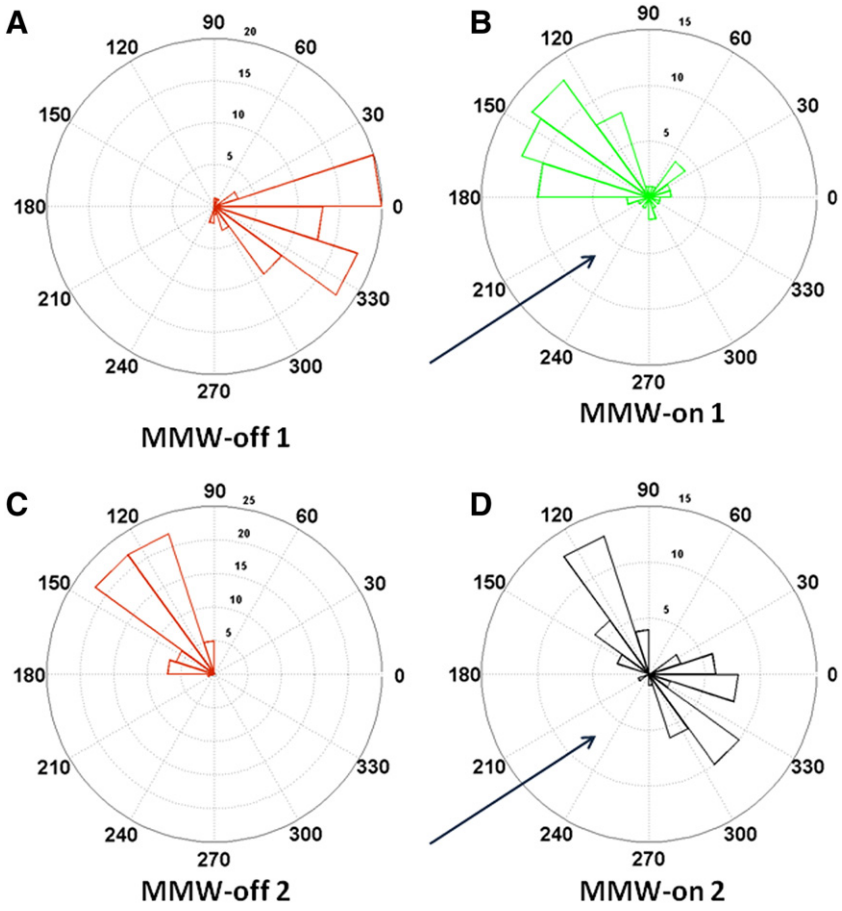

Fig. 9. Plots of angular histogram of the distribution of instantaneous angular values, showing the direction of vesicle motion in terms of relative frequency. A direction of 0° indicates +x motion where vector component runs parallel to the positive x-axis pointing to the right. A direction of 180° indicates −x motion 180° where vector component runs parallel to the negative x-axis pointing to the left. Arrows depict the position of MMW antenna.

top, bottom and sides of the dish. However, a very uniform distribution of SAR was present in the central region, covering an area of about 0.1 mm^2, where images of dispersed GVs were always acquired (Fig. 2C). An average SAR value of 0.2 W/kg was calculated in the observation section; this is far below the recommended SAR threshold value below which there is no significant temperature elevation that would cause bioeffects (0.2 W/kg vs. 1.6 W/kg) [37]. Notably, a negligible elevation of temperature is expected from this SAR level. As a matter of fact, an increase of 0.014 °C in temperature in 5 min of exposure is expected, in the worst case of absence of thermal conductive and convective exchanges, thus this intensity was so low that it could not cause local heating of the sample.

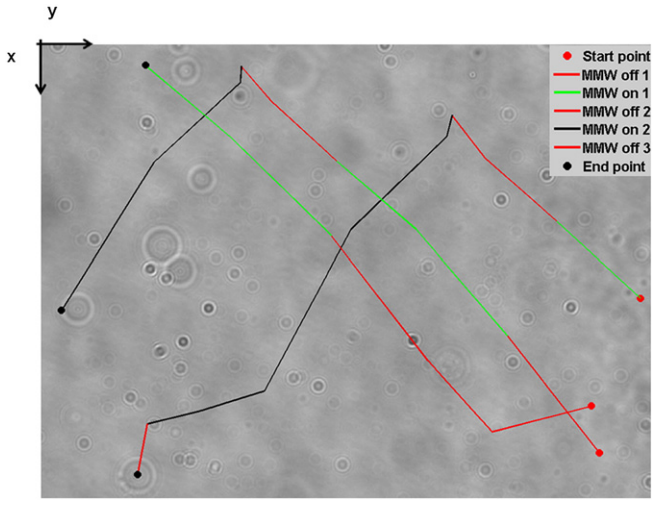

Fig. 10. Analysis of vesicle trajectory of negatively charged GVs subjected to interrupted regime of exposure. Eighteen microscope images were acquired and analyzed for the trajectories of three individual vesicles, vesicle diameters from 14 μm to 20 μm. The green and black segments exhibit MMW treatment and the red segment is sham condition. It should be noted that two of the three vesicles had moved out of the field of view.

4. Conclusions

Giant vesicles as cell-size system provide a very useful model system for investigating the effects of electromagnetic fields on lipid membranes. They allow for direct microscopy observation of membrane perturbations in the millimeter range. We examined specifically the motion of giant vesicles subjected to 53.37 GHz radiation when the GVs were randomly dispersed in the glucose solution at layers well below the upper surface of the liquid where vesicle motion induced by the onset of temperature spatial gradients was negligible. This was confirmed by the analysis of the motion of GVs under sham irradiation, which did not exhibit preferential direction. On the contrary, the irradiation induced a collective reorientation in the vesicles' motion. These changes occur only during irradiation with a “switch on” of the effect.

However, further experimental and theoretical studies are needed to increase our knowledge about the possibility to model an effective coupling between MMW radiation and charged structures in aqueous environments.

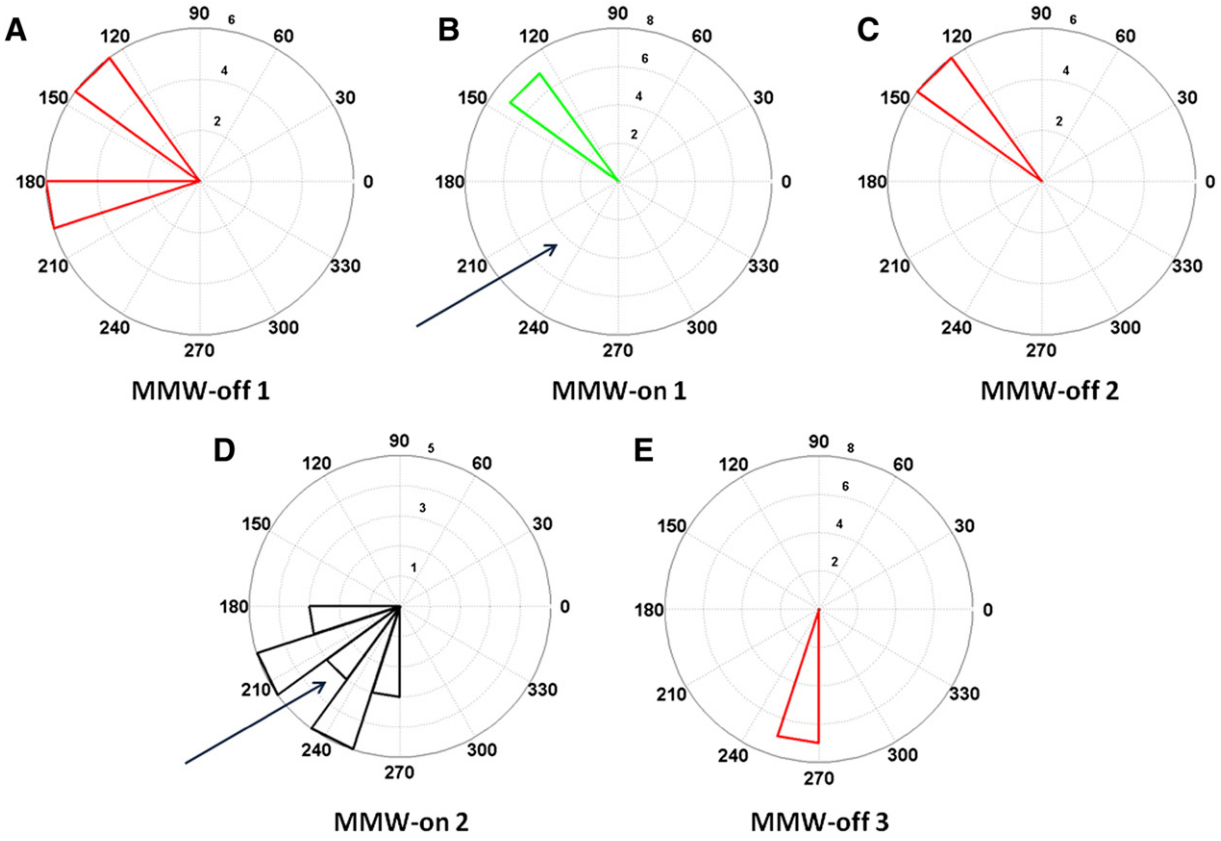

Fig. 11. Plot angular histogram of the distribution of instantaneous angular values, showing the direction of anionic vesicle motion, in terms of relative frequency. (A) Start MMW-off; vesicles migrate in the negative x-axis direction, maintaining angles on the second and third quadrant. (B) First MMW-on for short time: no relevant change in angular distribution. (C) Second MMW-off for short time: not at all change in angular distribution. (D) Second MMW-on: slight change of the angular distribution. (E) Third MMW-off: slight change of the angular distribution. Arrows depict the position of MMW antenna.

Acknowledgments

A.R.O. acknowledges with gratitude the financial support from Consiglio Nazionale delle Ricerche, Italy.

References

[1] M.A. Rojavin, M.C. Ziskin, Medical applications of millimeter waves, Int. J. Med. 91 (1998) 57–66.
[2] O.V. Betskii, N.D. Devyatkov, V.V. Kislov, Low intensity millimeter waves in medicine and biology, Crit. Rev. Biomed. Eng. 28 (2000) 247–268.
[3] A.G. Pakhomov, M.R. Murphy, Low-intensity millimeter waves as a novel therapeutic modality: nonthermal medical/biological treatments using electromagnetics waves and ionized gases, IEEE Trans. Plasma Sci. 28 (2000) 34–40.
[4] T.I. Usichenko, H. Edinger, V.V. Gizhko, C. Lehmann, M. Wendt, F. Feyerherd, Low-intensity electromagnetic millimeter waves for pain therapy, Evid. Based Complement. Alternat. Med. 3 (2006) 201–207.
[5] M.C. Ziskin, Physiological mechanisms underlying millimeter wave therapy, Bioelectromagnetics Current Concepts, NATO Security through Science Series, vol. 2006, Springer Netherlands Publ., 2006, pp. 241–251.
[6] V. Pikov, P.H. Siegel, Novel neural interface for modulation of neuronal activity based on millimeter wave exposure, Proceedings of the Life Science Systems and Applications Workshop (LiSSA); IEEE/NIH, 2011, pp. 147–151.
[7] S. Martel, Journey to the centre of a tumour, IEEE Spectr. 49 (2012) 43–47.
[8] T. Globus, D.L. Woolard, T. Khromova, T.W. Crowe, M. Bykhovskaya, B.L. Gelmont, et al., THz spectroscopy of biological molecules, J. Biol. Phys. 29 (2003) 89–100.
[9] M. Cifra, J.Z. Fields, A. Farhadi, Electromagnetic cellular interactions, Prog. Biophys. Mol. Biol. 105 (2011) 223–246.
[10] A. Ramundo-Orlando, G. Longo, M. Cappelli, M. Girasole, L. Tarricone, A. Beneduci, R. Massa, The response of giant phospholipid vesicles to millimetre waves radiation, BBA Biomembr. 1788 (2009) 1498–1507.
[11] L. Di Donato, M. Cataldo, P. Stano, R. Massa, A. Ramundo-Orlando, Permeability changes of cationic liposomes loaded with carbonic anhydrase induced by millimetre waves, Radiat. Res. 178 (2012) 437–446.
[12] I. Belayev, Non-thermal biological effects of microwaves, Microw. Rev. 11 (2005) 13–29.
[13] R. Dimova, C. Dietrich, B. Pouligny, Motion of particles attached to giant vesicles: falling ball viscosimetry and elasticity measurements on lipid membranes, in: P. Walde, P. Luisi (Eds.), Giant Vesicles, John Willey & Sons, Ltd., 1999, p. 221.
[14] J. Solon, P. Streicher, R. Richter, F. Brochard-Wyart, P. Bassereau, Vesicles surfing on a lipid bilayer: self-induced haptotactic motion, PNAS 103 (2006) 12382–12387.
[15] G. Danker, C. Verdier, C. Misbah, Dynamic and rheology of a dilute suspension of vesicles: higher order theory, J. Non-Newtonian Fluid Mech. 152 (2008) 156–167.
[16] T. Franke, R.H.W. Hoppe, C. Linsenmann, L. Schimd, C. Willbold, A. Wixforth, Numerical simulation of the motion of red blood cells and vesicles in microfluidics flow, Comput. Vis. Sci. 14 (2011) 167–180.
[17] N. Kuster, F. Schönborn, Recommended minimal requirements and development guidelines for exposure setups of bio-experiments addressing the health risk concern of wireless communications, Bioelectromagnetics 21 (2000) 508–514.
[18] D.J. Estes, M. Mayer, Electroformation of giant liposomes from spin-coated films of lipids, Colloids Surf. B: Biointerfaces 42 (2005) 115–123.
[19] C.A. Schneider, W.S. Rasband, K.W. Eliceiri, NIH Image to ImageJ: 25 years of image analysis, Nat. Methods 9 (2012) 671–675.
[20] W.J. Polacheck, J.L. Charest, R.D. Kamm, Interstitial flow influences direction of tumor cell migration through competing mechanisms, Proc. Natl. Acad. Sci. U. S. A. 108 (2011) 11115–11120.
[21] J.X. Zhao, Numerical dosimetry for cells under millimetre-wave irradiation using Petri dish exposure set-ups, Phys. Med. Biol. 50 (2005) 3405–3421.
[22] B.M. Garin, V.V. Meriakri, E.E. Chigrai, M.P. Parkhomenko, M.G. Akat'eva, Dielectric properties of water solutions with small content of glucose in the millimeter wave band and the determination of glucose in blood, PIERS Online 7 (2011) 555–558.
[23] N. Kishore, R.N. Goldberg, Y.B. Tewari, Apparent molar heat capacities and apparent molar volumes of aqueous glucose at temperatures from 298.15 K to 327.01 K, J. Chem. Thermodyn. 25 (1993) 847–859.
[24] P. Girard, P. Pecreaux, G. Lenoir, P. Falson, J.L. Rigaud, P. Bassereau, A new method for the reconstitution of membrane proteins in giant unilamellar vesicles, Biophys. J. 87 (2004) 419–429.
[25] E.P. Khizhnyak, M.C. Ziskin, Temperature oscillations in liquid media caused by CW millimeter wave electromagnetic irradiation, Bioelectromagnetics 17 (1996) 223–229.
[26] R. Darros-Barbosa, Temperature and concentration dependence of heat capacity of model aqueous solutions, Int. J. Food Prop. 6 (2007) 239–258.
[27] J. Schuderer, T. Samaras, W. Oesch, D. Spät, N. Kuster, High peak SAR exposure unit with tight exposure and environmental control for in vitro experiments at 1800 MHz, IEEE Trans. Microw. Theory Tech. 52 (2004) 2057–2066.

[28] J.X. Zhao, In vitro dosimetry and temperature evaluations of a typical millimeter-wave aperture-field exposure setup, IEEE Trans. Microw. Theory Tech. 60 (2012) 3608–3622.
[29] M. Mally, J. Majhene, S. Svetina, B. Zeks, The response of giant vesicles to pore-forming peptide melittin, Biochim. Biophys. Acta 1768 (2007) 1179–1189.
[30] I.R. Suárez, C. Leidy, G. Téllez, G. Gay, A. Gonzalez-Mancera, Slow sedimentation and deformability of charged lipid vesicles, PLoS ONE 8 (2013) e68309, http://dx.doi.org/10.1371/journal.pone.0068309.
[31] E. Evans, W. Rawicz, Entropy-driven tension and bending elasticity in condensed-fluid membranes, Phys. Rev. Lett. 64 (1990) 2094–2097, http://dx.doi.org/10.1103/physrevlett.64.209.
[32] P.M. Vlahovska, R.S. Gracia, S. Aranda-Espinoza, R. Dimova, Electrohydrodynamic model of vesicle deformation in alternating electric fields, Biophys. J. 96 (2009) 4789–4803.
[33] J.J. Seiwert, P.M. Vlahovska, Instability of a fluctuating membrane driven by an ac electric field, Phys. Rev. E. 87 (2013) 022713.
[34] R. Dimova, N. Bezlyepkina, M. Domange Jordo, R.L. Knorr, K.A. Riske, M. Staykova, P.M. Vlahovska, T. Yamamoto, P. Yang, R. Lipowsky, Vesicles in electric fields: some novel aspects of membrane behavior, Soft Matter 5 (2009) 3201–3212.
[35] Y.P. Chukova, Doubts about nonthermal effects of MM radation have no scientific foundations, J. Phys. Conf. Ser. 329 (2011) 012032.
[36] T. Takahashi, F. Nomura, Y. Yokoyama, Y. Tanaka-Takiguchi, M. Homma, K. Takiguchi, Multiple membrane interactions and versatile vesicle deformations elicited by melittin, Toxins 5 (2013) 637–664.
[37] IEEE Standard for safety levels with respect to human exposure to radiofrequency electromagnetic fields, 3 kHz to 300 GHz, IEEE Standard C95.1, 2005.